RSC Advances

PAPER

View Article Online
View Journal | View Issue

Cite this: *RSC Adv.*, 2020, **10**, 9525

Synthesis of the diketopyrrolopyrrole/terpyridine substituted carbazole derivative based polythiophenes for photovoltaic cells†

Shih-Hao Wang,[a] Teng-Wei Wang,[a] Hsieh-Chih Tsai,[bc] Po-Chih Yang,[d] Chih-Feng Huang[a] and Rong-Ho Lee*[a]

Received 19th November 2019
Accepted 13th February 2020

DOI: 10.1039/c9ra09649c

rsc.li/rsc-advances

A series of conjugated polythiophenes (PTs) having low band gap energies (**PDPP**, **PDPCz21**, **PDPCz11**), with 2-ethylhexyl-functionalized 2,5-thienyl diketopyrrolopyrrole (TDPP) as the electron acceptor and terpyridine-substituted carbazole (TPCz) as the electron donor, have been synthesized and studied for their applicability in polymer-based photovoltaic cells (PVCs). The thermal stability and solvent solubility of PTs increased upon increasing the content of the TPCz derivative. PVCs were fabricated having the following architecture: indium tin oxide/poly(3,4-ethylenedioxythiophene):polystyrenesulfonate/PT:6,6-phenyl-C_{71}-butyric acid methyl ester ($PC_{71}BM$)/Ca/Ag. The compatibility between the PT and $PC_{71}BM$ improved upon increasing the TPCz content. The photovoltaic properties of the **PDPCz21**-based PVCs were superior to those of their **PDPP**- and **PDPCz11**-based counterparts.

1. Introduction

Because of their light weight, low cost, and flexibility, π-conjugated polythiophenes (PTs) are promising candidates for various optoelectronic device applications, including polymer light-emitting devices,[1,2] electrochromic devices,[3] organic field-effect transistors,[4,5] photovoltaic (PV) cells,[6–15] and fluorescent chemosensors.[16–19] Polymer-based photovoltaic cells (PVCs) typically contain a layer comprising a blend of PT and a fullerene derivative.[20] The illumination of PVC creates excitons, which separate at the interface between the PT and the fullerene derivative.[21] The resulting electrons and holes are transported through the electron-acceptor and -donor phases, respectively, to the cathode and anode of the cell.[22] An effective PVC requires a PT to have a high degree of photo-absorption, high charge mobility, and suitable lowest unoccupied molecular orbital (LUMO) and highest occupied molecular orbital (HOMO) energy levels.[23] The PT should have low band gap energy to ensure the harvesting of a large amount of solar radiation. Moreover, it should exhibit high charge mobility to ensure a high current density in the PVC.[24] Ideally, the morphology of the photoenergy conversion layer should feature phase separation at the nanoscale, along with a large interfacial area between the PTs and fullerene derivative, thereby enhancing the exciton dissociation, electron and hole transfer, and charge collection at the electrodes.[25]

Many PVCs displaying good PV performance have featured PTs containing electron-donor and -acceptor (D–A)-type structures.[26–28] Such electron- and hole-transporting segments are responsible for a broader range of light absorption and the higher electron and hole mobilities of the resulting photoenergy conversion layers and, therefore, the enhanced PV performance of the PVCs.[29–31] Triphenylamine (TPA) and carbazole derivatives are among the most popular electron donor groups because of their good electron-donating and hole-transporting performance and their good solubility in the organic solvents.[32,33] Several electron-deficient moieties, including perylenediimide, benzothiadiazole, and diketopyrrolopyrrole (DPP) units, have been incorporated into the backbones of polymers to be the electron-withdrawing and -transporting units.[34–37] In particular, the DPP derivatives have been major components in the D–A-type PTs used in PVCs.[38–41] The DPP-containing polymers often possess low band gap energies because of their strong electron-accepting properties, thereby extending their light-absorption range to 800–900 nm.[42–44] Furthermore, the high tendency of these polymers to crystallize enables them to provide high charge carrier mobilities.[27] In addition, the pyridine-flanked DPP-based conjugated polymers possess lower energy levels and more planar structures, favoring their use as electron-transporting polymers.[45] Moreover, the pyridine-flanked asymmetric DPP-based copolymers have also been reported for PVCs.[46] The

[a]*Department of Chemical Engineering, National Chung Hsing University, Taichung 402, Taiwan. E-mail: rhl@nchu.edu.tw; Fax: +886-4-22854734; Tel: +886-4-22854308*
[b]*Graduate Institute of Applied Sci. and Tech., National Taiwan University of Science and Technology, Taipei 10607, Taiwan*
[c]*Advanced Membrane Materials Center, National Taiwan University of Science and Technology, Taipei 10607, Taiwan*
[d]*Department of Chemical Engineering and Materials Science, Yuan Ze University, Taoyuan City 320, Taiwan*

† Electronic supplementary information (ESI) available. See DOI: 10.1039/c9ra09649c

more planar structures of these conjugated polymers result from the lower steric bulk of the nitrogen atoms in the pyridine moieties. Consequently, higher PV efficiencies have been observed for PVCs incorporating pyridine-flanked DPP polymers. For example, Qiu *et al.* reported an asymmetric thiophene/pyridine-flanked DPP polymer (PyTDPP) that exhibited a narrow band gap, a wide light absorption range, and a relatively deep HOMO; PyTDPP-based PVCs displayed high PV efficiency.[47] Furthermore, Chen *et al.* synthesized two terpyridine-functionalized DPP derivatives;[48] directed by zinc(II) and cadmium(II) ions, these DPP derivatives underwent polymerization to form metallo-supramolecular polymers, which exhibited low band gap energies (1.51–1.58 eV) and broad absorption bands (ranging from *ca.* 300 to 800 nm), suggesting potential applications in high-performance PV materials.

To expand upon these ideas, in this study, three D–A-type PTs (**PDPP**, **PDPCz21**, **PDPCz11**), featuring 2-ethylhexyl-functionalized 2,5-thienyl diketopyrrolopyrrole (TDPP) moiety as the electron acceptor and terpyridine-substituted carbazole (TPCz) moiety as the electron donor, were synthesized and studied for their PV properties in PVCs. The presence of TDPP units in the polymer backbone can enhance the absorption edge to wavelengths of up to 1000 nm.[42,44,49] Unfortunately, increasing the TDPP content decreases the solubility of the polymers due to increased degrees of π-stacking among the polymer chains. The PV properties of such polymer-based PVCs are moderate.[42,49] Moreover, lower band gap energies and higher charge mobilities were expected for PTs (**PDPCz21**, **PDPCz11**) having TPCz- and TDPP-based bipolar characteristics, potentially enhancing the PV efficiencies of PVCs. Furthermore, the electron-withdrawing terpyridine-substituted carbazole TPCz is a D–A-type conjugated pendant. PT derivatives bearing D–A-type TPCz-conjugated pendant units absorb broadly in the UV and visible regions and can, therefore, harvest greater amounts of solar light. The presence of D–A-type conjugated pendants can also improve the charge mobilities of the polymers. In addition, we expected to observe enhanced solubility for PTs presenting pendent terpyridine units and for the electron-rich nitrogen atoms of the terpyridine units to interact strongly with the C=O group of $PC_{71}BM$, thereby increasing the compatibility between PT and the fullerene derivative. Furthermore, we expected the presence of bulky pendants to increase the miscibility of the PT and the fullerene derivative because the bulky pendant units would provide sufficient volume for the fullerene derivative to intercalate within the polymer segments.[50] PVCs were fabricated based on a blend of each PT with polythiophene:6,6-phenyl-C_{71}-butyric acid methyl ester ($PC_{71}BM$). According to the PV performances of these PVCs, the influence of the TPCz content in our PTs was determined.

2. Experimental section

2.1 Chemicals

Tetrakis(triphenylphosphine)palladium(0) [$Pd(PPh_3)_4$], potassium carbonate (K_2CO_3), copper iodide (CuI), and other organic reagents were purchased from Alfa, Aldrich, TCI, and Acros, and used without purification. Dichloromethane (DCM), toluene, *o*-dichlorobenzene (*o*-DCB), and dimethylformamide (DMF) were freshly distilled over drying agents, then purged with nitrogen, prior to use. According to procedures reported in the literature, 4′-(4-bromophenyl)-2-2′:6′,2″-terpyridine (**1**), 3,6-di(2-bromothien-5-yl)-2,5-di(2-ethylhexyl)pyrrolo[3,4-*c*]pyrrole-1,4-dione (**3**), and 2,5-bis(trimethylstannyl)thiophene (**4**) were synthesized.[18,28,51] The syntheses of 3,6-dibromo-9-(4-[2,6-di(pyrid-2-yl) pyrid-4-yl]phenyl)-9*H*-carbazole (**2**) and the PTs **PDPP**, **PDPCz21**, and **PDPCz11** are presented in Scheme 1.

2.2 Synthesis

Compound 2. A mixture of compound **1** (0.970 g, 2.50 mmol), 3,6-dibromocarbazole (1.22 g, 3.75 mmol), K_2CO_3 (1.38 g, 10.0 mmol),[18] crown-6 (0.330 g, 1.25 mmol), and CuI (0.480 g, 2.50 mmol) in dry DMF (50 mL) was stirred at 150 °C under N_2 for 24 h. After cooling to 25 °C, the mixture was partitioned between water and DCM. The organic phase was concentrated to dryness. The solid product was recrystallized (DCM/MeOH) to provide a yellow solid (0.52 g, 33%). ^{1}H NMR (δ/ppm, 600 MHz, $CDCl_3$): 7.31 (d, 2H), 7.37 (t, 2H), 7.52 (d, 2H), 7.63 (d, 2H), 7.91 (t, 2H), 8.19 (s, 2H), 8.68 (d, 2H), 8.73 (d, 2H), 8.81 (s, 2H), 8.83 (d, 2H). Anal. calcd for $C_{33}H_{20}N_4Br_2$: C, 62.66; H, 3.16; N, 8.86; Br, 25.32. Found: C, 62.63; H, 3.17; N, 8.85; Br, 25.35.

PDPP. A solution of **3** (1.54 g, 2.50 mmol), **4** (1.33 g, 2.50 mmol), and $Pd(PPh_3)_4$ (0.300 g, 0.250 mmol) in toluene (30 mL) was stirred under reflux for 2 days, and was then poured into MeOH (100 mL). The precipitated solid was filtered into a Soxhlet thimble and extracted with acetone, MeOH, and DCM. The polymer **PDPP** was obtained from the DCM fraction through rotary evaporation. A deep-blue polymer (0.86 g, 30%) was obtained after drying under vacuum. ^{1}H NMR (δ/ppm, 600 MHz, CD_2Cl_2): 0.77–0.94 (m, 6H), 1.18–1.41 (m, 16H), 1.82–1.92 (m, 2H), 4.04 (s, 4H), 7.04 (d, 2H), 7.31 (d, 2H), 7.42 (d, 2H), 7.63 (d, 2H), 8.90 (d, 2H), 8.93–8.95 (d, 2H). Anal. calcd for ($C_{34}H_{40}N_2O_2S_3$): C, 67.55; H, 6.62; N, 4.64; O, 5.30; S, 15.89. Found: C, 67.51; H, 6.64; N, 4.68; O, 5.27; S, 15.90.

PDPCz21. A mixture of **2** (1.43 g, 2.50 mmol), **3** (1.51 g, 2.50 mmol), **4** (2.05 g, 5.00 mmol), and $Pd(PPh_3)_4$ (0.300 g, 0.250 mmol) in dry toluene (30 mL) was stirred under reflux for 2 days, and was then poured into MeOH (100 mL). The precipitated crude product was filtered into a Soxhlet thimble and extracted with acetone, MeOH, and DCM. The polymer was obtained from the DCM fraction through rotary evaporation. A deep-blue polymer (0.41 g, 28%) was obtained after drying under vacuum. ^{1}H NMR (δ/ppm, 600 MHz, CD_2Cl_2): 0.67–0.97 (m, 26H), 1.15–1.42 (m, 70H), 1.81–1.95 (s, 4H), 3.92–4.13 (s, 9H), 6.80–8.40 (m, 32H), 8.7–9.0 (m, 12H). Anal. calcd for [($C_{34}H_{40}N_2O_2S_3$)$_{2.2}$($C_{37}H_{22}N_4S$)$_{1.0}$]: C, 71.26; H, 5.84; N, 6.24; O, 3.74; S, 12.92. Found: C, 71.29; H, 5.82; N, 6.22; O, 3.78; S, 12.89.

PDPCz11. A mixture of **2** (2.15 g, 3.75 mmol), **3** (1.51 g, 2.50 mmol), **4** (2.05 g, 5.00 mmol), and $Pd(PPh_3)_4$ (0.300 g, 0.250 mmol) in dry toluene (30 mL) was stirred under reflux for 2 days, and was then poured into MeOH (100 mL). The precipitated crude product was filtered into a Soxhlet thimble and extracted with acetone, MeOH, and DCM. The polymer was obtained from the DCM fraction through rotary

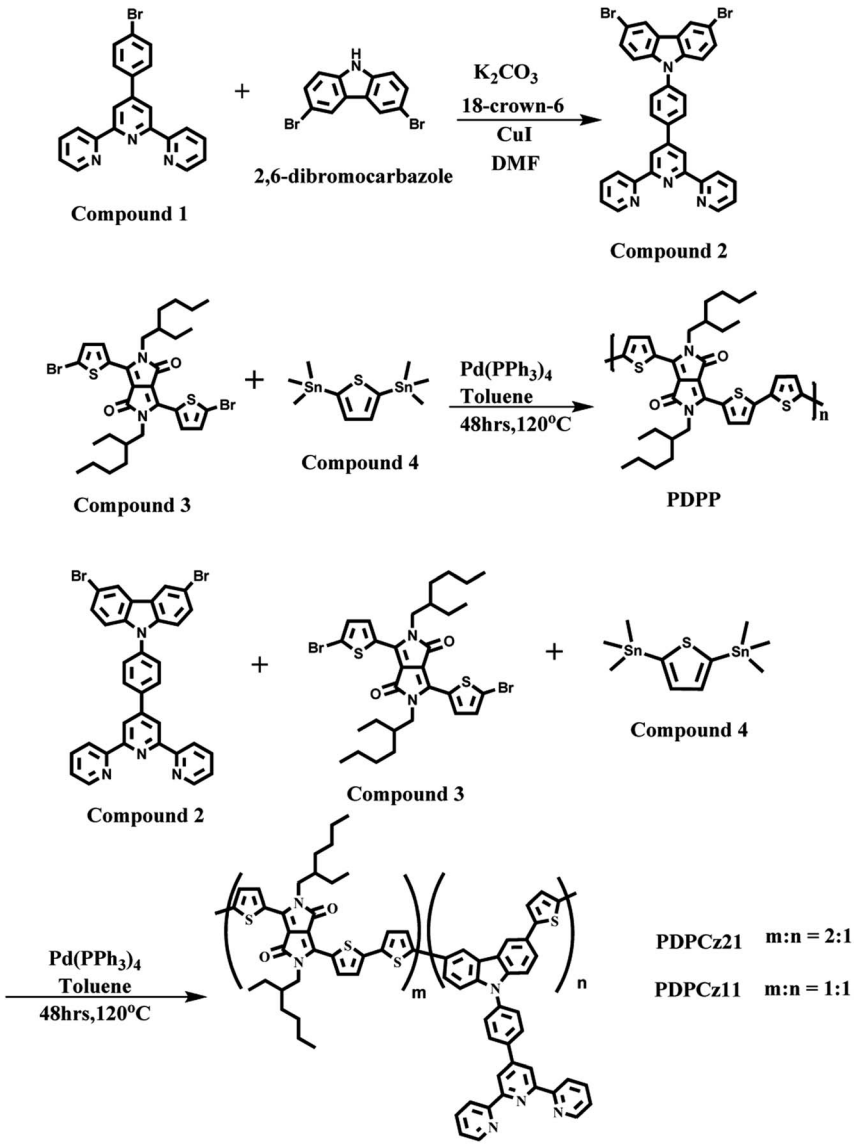

Scheme 1 Synthesis of PDPP, PDCz21, and PDCz11.

evaporation. A deep-blue polymer (0.46 g, 32%) was obtained after drying under vacuum. ^{1}H NMR (δ/ppm, 600 MHz, CD_2Cl_2): 0.67–0.97 (m, 12H), 1.15–1.42 (m, 16H), 1.81–1.95 (s, 2H), 3.92–4.13 (s, 4H), 6.80–8.40 (m, 18H), 8.7–9.0 (m, 10H). Anal. calcd for $[(C_{34}H_{40}N_2O_2S_3)_{1.1}(C_{37}H_{22}N_4S)_{1.0}]$: C, 73.28; H, 5.42; N, 7.12; O, 2.89; S, 11.29. Found: C, 73.32; H, 5.36; N, 7.15; O, 2.94; S, 11.23.

2.3 Characterization of PTs

The ^{1}H NMR spectra of PTs were recorded on a Varian Unity Inova spectrometer (600 MHz). The number-average molecular weights (M_n) and weight-average molecular weights (M_w) of PTs were measured through gel permeation chromatography (GPC) by using the Waters chromatography system (717 plus Autosampler) equipped with two Waters Styragel linear columns; polystyrene (PS) standards were employed, with tetrahydrofuran (THF) as the eluent. The glass transition temperatures (T_g) of PTs were studied through differential scanning calorimetry (DSC; TA Instruments, DSC-2010). The thermal degradation temperatures (T_d) of PTs were measured through thermogravimetric analysis (TGA; TA Instruments, TGA-2050). Both DSC and TGA analyses were performed under the N_2 atmosphere with a scanning rate of 10 °C min^{-1}. A Hitachi U3010 UV-Vis spectrometer was used to record the UV-Vis absorption spectra of PTs. Cyclic voltammetry (CV) of PTs was performed using a CHI 611D electrochemical analyzer (scanning rate: 50 mV s^{-1}) equipped with Pt electrodes and an Ag/Ag$^+$ (0.10 M $AgNO_3$ in MeCN) reference electrode in an anhydrous, N_2-saturated solution of 0.1 M Bu_4NClO_4 in MeCN. Bu_4NClO_4 (98%, TCI) was recrystallized three times from MeOH/water (1 : 1) and then dried at 100 °C under vacuum. A Pt plate coated with a thin film of PT was used as the working electrode; a Pt wire was used as the counter electrode, and an Ag/Ag$^+$ electrode was used as the reference electrode. The electrochemical potential was calibrated against ferrocene/

ferrocenium. Atomic force microscopy (AFM; Seiko SII SPA400; tapping mode) and transmission electron microscopy (TEM; JEOL JEM-1400) were used to investigate the morphologies of the PT/$PC_{71}BM$ composite films.

2.4 PVC fabrication and characterization

The PVCs had the following architecture: indium tin oxide (ITO)-coated glass/hole transporting material (HTM)/photoenergy conversion layer/Ca (10 nm)/Ag (100 nm), where the photoenergy conversion layer comprised an interpenetrating network of PT and $PC_{71}BM$. The ITO-coated glass was purchased from Applied Film Corp. $PC_{71}BM$ was purchased from Nanocarbon Corp. and used without further purification. The PVCs were fabricated as follows: the ITO coated glass substrates were washed well and then cleaned through O_2 plasma treatment. An HTM layer comprising poly(3,4-ethylenedioxythiophene) doped with polystyrenesulfonate (PEDOT:PSS; AI4083, Heraeus Clevios) was coated on the ITO layer through spin-coating. The sample was dried at 140 °C for 20 min. A PT/$PC_{71}BM$ solution (30 mg mL^{-1} in *o*-DCB) was stirred for 12 h, then filtered through a 0.2 μm polytetrafluoroethylene filter and spin-coated (2000 rpm, 60 s) onto the PEDOT:PSS layer to fabricate the photoenergy conversion layer. The sample was thermally treated at 100 °C for 10 min in an N_2-filled glove box. The Ca/Ag-based cathode was thermally deposited onto the photoenergy conversion layer in a high-vacuum chamber. The photoenergy conversion area of the PVC was 0.04 cm^2. The PVC was encapsulated with epoxy resin. A quartz thickness monitor (STM-100/MF, Sycon) was used to determine the deposition rate of the Ca/Ag cathode. A surface texture analysis system (3030ST, Dektak) was used to confirm the thicknesses of the photoenergy conversion layer. The PV properties of the PT-based PVCs were measured using a programmable electrometer equipped with current and voltage sources (Keithley 2400) under illumination with solar-simulating light (100 mW cm^{-2}) from an AM1.5 solar simulator (NewPort Oriel 96000).

3. Results and discussion

3.1 Characterization of PTs

The PTs **PDPP**, **PDPCz21**, and **PDPCz11** were prepared through Stille coupling polymerization of compounds **2**, **3**, and 2,5-bis(trimethylstannyl)thiophene (**4**). The ^1H NMR spectra of **PDPP**, **PDPCz21**, and **PDPCz11** are presented in Fig. S1–S3,† respectively. The chemical shifts and signal intensities of the peaks in the ^1H NMR spectra were in agreement with the proposed chemical structures of PTs. The **PDPCz21** and **PDPCz11** polymers with different TDPP/TPCz ratios (*m*/*n*) were prepared by controlling the feed molar ratio of compounds **2**, **3**, and 2,5-bis(trimethylstannyl)thiophene (**4**). For **PDPCz21** and **PDPCz11**, the actual values of *m*/*n* (*ca.* 2.2 : 1 and 1.1 : 1, respectively) were determined from the relative integral areas of the peaks in the range of 6.80–9.10 ppm (representing protons of the vinylene, phenyl, and thiophene groups) and 0.60–4.20 ppm (representing protons of the ethylhexyl groups) in their ^1H NMR spectra. The values of M_n and M_w of PTs were determined through GPC to be in the range of 32.6–36.1 and 48.9–57.7 kg mol^{-1}, respectively (Table 1). High average molecular weights were obtained for PTs. In addition, the three PTs were soluble in DCM, THF, $CHCl_3$, cyclohexanone, and *o*-DCB. The good solubility favors the solution-processing of PT-based photoenergy conversion layers.

The values of T_g and T_d of PTs were measured through DSC and TGA (Table 1). The values of T_d for **PDPP**, **PDPCz21**, and **PDPCz11** were determined to be 350.6, 385.4, and 390.5 °C, respectively. Thus, the thermal stability of these PTs increased upon increasing the TPCz content, revealing the relatively poor thermal stability of TDPP. Moreover, the values of T_g for **PDPP**, **PDPCz21**, and **PDPCz11** were found to be 149.1, 150.5, and 170.6 °C, respectively. These high values of T_g for PTs suggested that they all would be suitable for the PVC applications. A relatively lower value of T_g was observed for **PDPP**, which had a higher content of flexible ethylhexyl-substituted TDPP moieties. In addition, a single endothermic glass transition was observed for each PT, implying that the TPCz and TDPP moieties were distributed homogeneously.

3.2 Optical absorption properties of PTs

The UV-Vis absorption spectra of DPP-containing PTs **PDPP**, **PDPCz21**, and **PDPCz11** were recorded as solutions in *o*-DCB and as thin films (Fig. 1). Their photophysical properties are summarized in Table 2. The wavelengths of light absorbed by the TDPP-based PTs in *o*-DCB ranged from 375 to 860 nm. Two broad absorption bands were observed for each PT. The first absorption band observed in the range of 375–475 nm was attributed to the n–π* transitions of the PT pendants and the π–π* transitions of the PT backbone.[52] In the range of 475–860 nm, the second absorption band was contributed by the intramolecular charge transfer (ICT) between the TPCz- and TDPP-based segments.[32] Relative to **PDPP**, the maximal absorption wavelengths of **PDPCz21** and **PDPCz11** in solution were blue-shifted due to the incorporation of the TPCz-based unit, suggesting a larger band gap energy for the TPCz moiety. Moreover, the presence of bulky side units usually results in the twisting of a polymer backbone. As a result, the conjugation length and the maximal absorption wavelength of PTs both decreased upon increasing the content of bulky side units.[32] On the other hand, the maximal absorption wavelengths of PTs in their solid film forms were greater than those in the solution due to strong π-stacking interactions between PT backbones

Table 1 The average molecular weights and thermal properties of PTs

PT	M_n (kg mol^{-1})	M_w (kg mol^{-1})	T_g[a] (°C)	T_d[b] (°C)
PDPP	35.5	51.8	149.1	350.6
PDPCz21	32.6	48.9	150.5	385.4
PDPCz11	36.1	57.7	170.6	390.5

[a] T_g: measured at a heating rate of 10 °C min^{-1}. [b] T_d: temperature at which weight loss reached 10%.

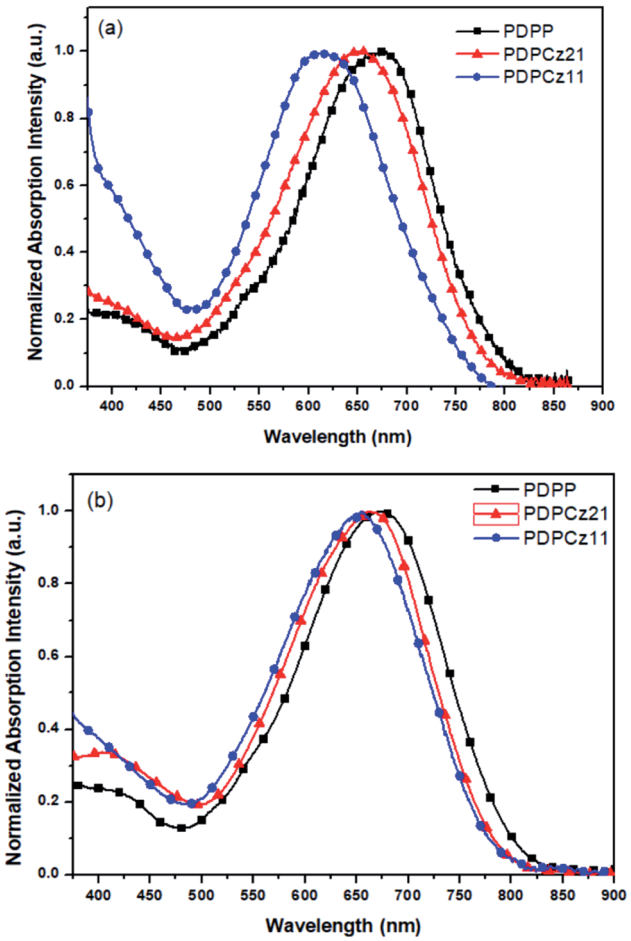

Fig. 1 The normalized UV-Vis absorption spectra of the PTs (a) in *o*-DCB solution and (b) as thin solid films.

and the pendants.[32] The band gap energies (E_g) of PTs in their forms as thin solid films were determined from the onset wavelengths of their light absorption bands. Table 2 reveals that the values of E_g for **PDPP**, **PDPCz21**, and **PDPCz11** were 1.45, 1.50, and 1.52 eV, respectively. Thus, the higher values of E_g resulted in PTs having higher TPCz contents.

The light absorption properties of the PT/$PC_{71}BM$ composite films are displayed in Fig. 2. The light absorption bands of the TDPP-containing PTs ranged from 375 to 860 nm. The maximum absorption peaks of PT appeared near 670 nm. Moreover, for these PT/$PC_{71}BM$ composite films, the absorption intensity of PT decreased upon increasing the $PC_{71}BM$ content. In terms of photon absorption, employing a lower amount of $PC_{71}BM$ in the photoenergy conversion layer is preferred. The typical stoichiometries of PT/$PC_{71}BM$ composites, optimal for PVCs in several PT systems, range from 1 : 1 to 1 : 4 (by weight).[32] A high proportion of $PC_{71}BM$ decreases the light absorption in the photoenergy conversion layer due to the poor light absorption of $PC_{71}BM$ in the visible region.

3.3 Electrochemical properties of PTs

Because the PV performance of PVC is related to the electrochemical properties of PT, CV was used to study the electrochemical properties of the TDPP/TPCz-based PTs and to estimate their HOMO energy levels. The oxidation peak of PTs was observed in the CV curves (Fig. 3). The oxidation potentials (E_{on}^{ox}) and the LUMO and HOMO energy levels of PTs are summarized in Table 2. The values of E_{on}^{ox} of **PDPP**, **PDPCz21**, and **PDPCz11** were found to be 0.64, 0.70, and 0.75 V, respectively. The presence of the electron-withdrawing terpyridine units decreased the oxidation ability of the TPCz moieties in the PT main chain. Therefore, the intensity of the oxidation peak decreased significantly for **PDPCz11**. Moreover, the value of E_{on}^{ox} of PTs increased upon increasing the TPCz content. Based on the values of E_{on}^{ox}, the HOMO energy levels of PTs were calculated according to the equation:

$$\text{HOMO} = -e(E_{on}^{ox} - E_{on,ferrocene}^{ox} + 4.80)\ (\text{eV})$$

where 4.80 eV is the energy level of ferrocene below the vacuum level. The value of E_{on}^{ox} of ferrocene/ferrocene$^+$ is 0.09 V in 0.1 M Bu_4NClO_4/MeCN. The HOMO energy levels obtained for **PDPP**, **PDPCz21**, and **PDPCz11** were −5.44, −5.50, and −5.55 eV, respectively. Additionally, the LUMO energy levels were estimated from the HOMO energy levels and the values of E_g (determined from the light absorption spectra) using the equation:

$$\text{LUMO} = \text{HOMO} + E_g\ (\text{eV})$$

The calculated LUMO energy levels were −3.99 eV for **PDPP**, −4.00 eV for **PDPCz21**, and –4.03 eV for **PDPCz11**. Thus, the lower LUMO energy levels were obtained for PTs having higher TPCz contents. Thus, the electrochemical behavior of these PTs could be tuned by varying the TPCz content in the PT backbone. The PV performance of a PVC is typically related to the HOMO energy level of its p-type PT. High open-circuit voltages (V_{OC}) are usually obtained for PVCs based on PTs having low HOMO energy levels.[32]

Table 2 The optical properties and electrochemical behavior of the PTs

PT	$\lambda_{max}^{abs\ a}$ (nm)	$\lambda_{max}^{abs\ b}$ (nm)	λ_{onset} (nm)	E_g^{optc} (eV)	E_{on}^{ox} (V)	LUMO (eV)	HOMO (eV)
PDPP	676	674	853	1.45	0.64	−3.99	−5.44
PDPCz21	651	663	828	1.50	0.70	−4.00	−5.50
PDPCz11	618	655	814	1.52	0.75	−4.03	−5.55

[a] Maximum absorption wavelength of the polymer in solution. [b] Maximum absorption wavelength of the polymer as a thin film. [c] Value of E_g calculated from the onset absorption (λ_{onset}^{abs}) of the polymer thin film: $E_g = 1240/\lambda_{onset}$.

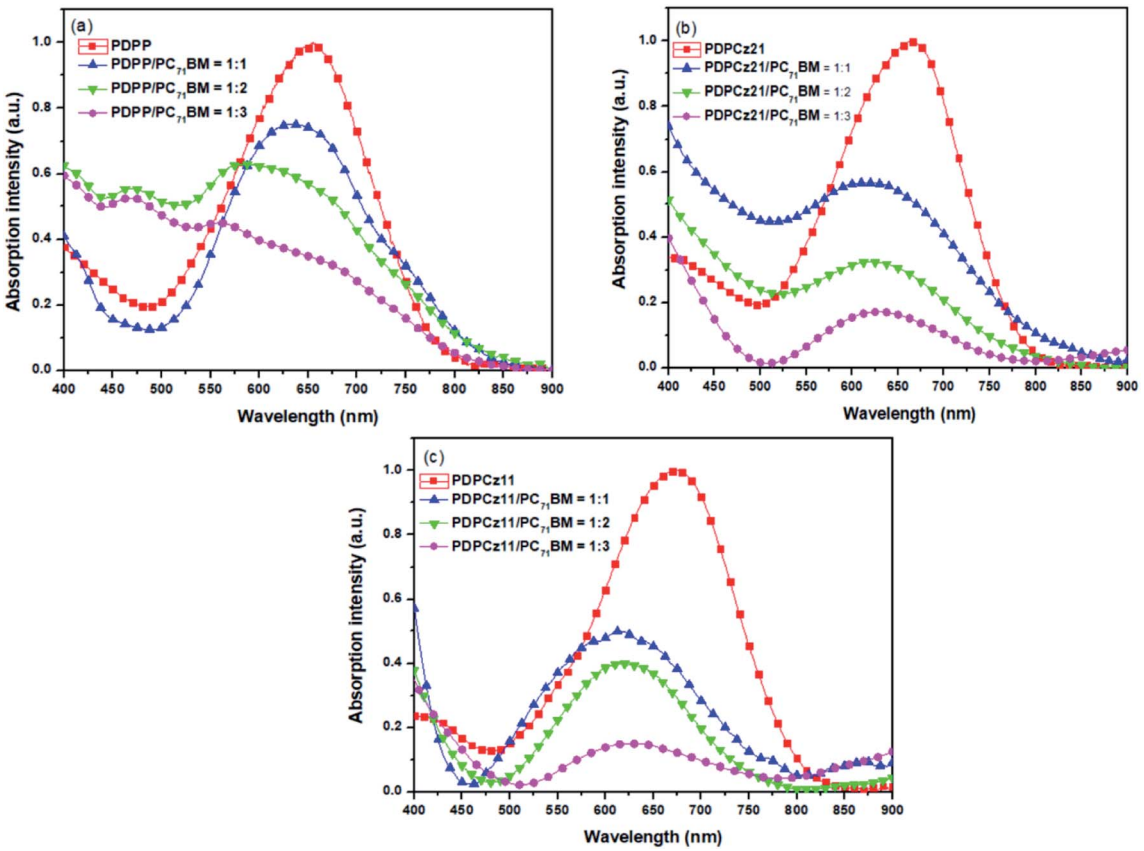

Fig. 2 The UV-Vis absorption spectra of (a) **PDPP**/$PC_{71}BM$, (b) **PDPCz21**/$PC_{71}BM$, and (c) **PDPCz11**/$PC_{71}BM$ blend films.

3.4 Morphologies of PT/$PC_{71}BM$-based thin films

The PV properties of PVC are closely related to the morphology of its PT/$PC_{71}BM$ blend film. To decrease the recombination of excitons, a P/N heterojunction phase must be fabricated at the nanoscale level.[25,32,50] AFM was used to study the compatibilities and morphologies of the PT/$PC_{71}BM$ solid films. Fig. 4–6 present the topographic and phase images of the **PDPP**/$PC_{71}BM$, **PDPCz21**/$PC_{71}BM$, and **PDPCz11**/$PC_{71}BM$ composite films, respectively, after their thermal treatment at 100 °C for 10 min. In Fig. 4, the AFM images reveal that the $PC_{71}BM$ units were not distributed uniformly in the **PDPP** film. The quality of the thin films of the **PDPP**/$PC_{71}BM$ blend films was poor, suggesting a high degree of π-stacking of the TDPP moieties in the PT main chain, consistent with the relatively low solubility of **PDPP**. In contrast, the AFM images of the **PDPCz21**/$PC_{71}BM$ and **PDPCz11**/$PC_{71}BM$ composite films revealed uniform distributions of $PC_{71}BM$ in PTs. Accordingly, the **PDPCz21** and **PDPCz11** composite films were of good quality. Thus, the compatibility of PT and $PC_{71}BM$ was enhanced after the addition of TPCz units into the PT backbone. Incorporating bulky pendants increased the free volume of the PT backbone and, subsequently, enhanced the compatibility of PT and $PC_{71}BM$.[49] Consequently, the phase-separated interpenetrating networks with $PC_{71}BM$-based sizable domains were observed for the **PDPCz21**/$PC_{71}BM$ and **PDPCz11**/$PC_{71}BM$ composites. Some degree of phase separation was important for the efficient formation of free carriers to provide PVCs with optimal PV properties. Nanoscale phase separation was more obvious for the **PDPCz21**/$PC_{71}BM$ [1 : 1, 1 : 2, and 1 : 3 (w/w)] and **PDPCz11**/$PC_{71}BM$ [1 : 2 and 1 : 3 (w/w)] blend films. Moreover, the morphology of the **PDPCz11**/$PC_{71}BM$ (1 : 1, w/w) blend solid film [Fig. 6(a)] was more homogeneous than that of the **PDPCz21**/$PC_{71}BM$ (1 : 1, w/w) composite solid film [Fig. 5(a)], presumably because **PDPCz11** possessed a higher content of TPCz groups and, thereby, displayed enhanced compatibility with $PC_{71}BM$.

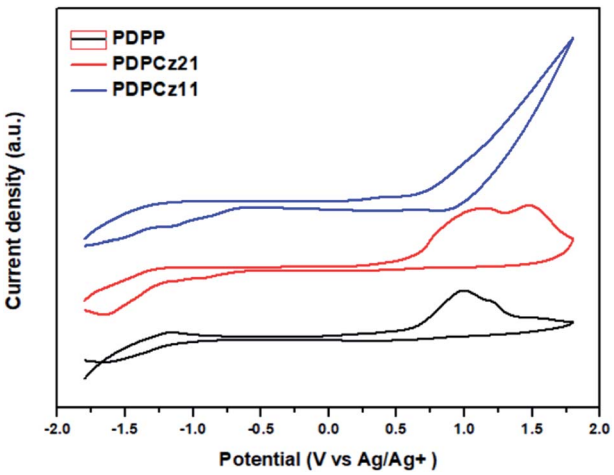

Fig. 3 Cyclic voltammograms of PDPP, PDPCz21, and PDPCz11.

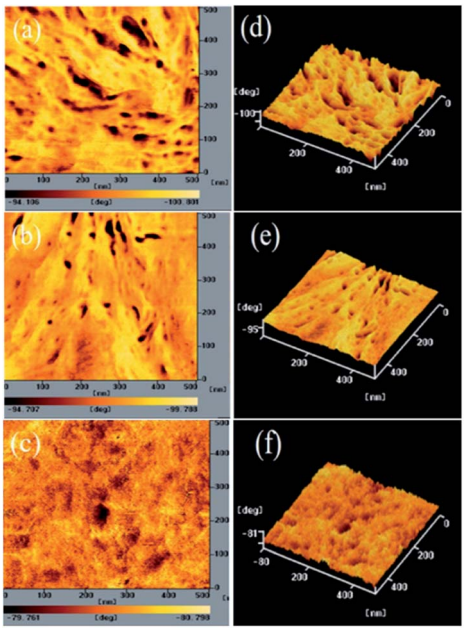

Fig. 4 AFM (tapping mode) (a–c) phase and (d–f) topographic images of **PDPP**/$PC_{71}BM$ blend films [(a and d) 1 : 1, w/w; (b and e) 1 : 2, w/w; (c and f) 1 : 3, w/w], recorded after annealing at 100 °C for 10 min.

The TEM images were recorded to further study the distribution of $PC_{71}BM$ in the blend films. The TEM images of the **PDPCz21**/$PC_{71}BM$ blends films [1 : 1, 1 : 2, and 1 : 3 (w/w)] are displayed in Fig. 7. The dark areas in the TEM images represent the $PC_{71}BM$ domains (the electron-scattering density of $PC_{71}BM$ was greater than that of PTs). The phase-separated

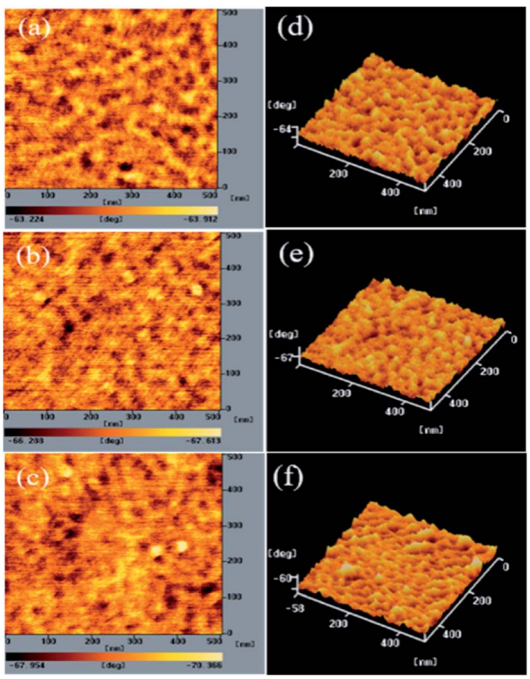

Fig. 5 AFM (tapping mode) (a–c) phase and (d–f) topographic images of **PDPCz21**/$PC_{71}BM$ blend films [(a and d) 1 : 1, w/w; (b and e) 1 : 2, w/w; (c and f) 1 : 3, w/w], recorded after annealing at 100 °C for 10 min.

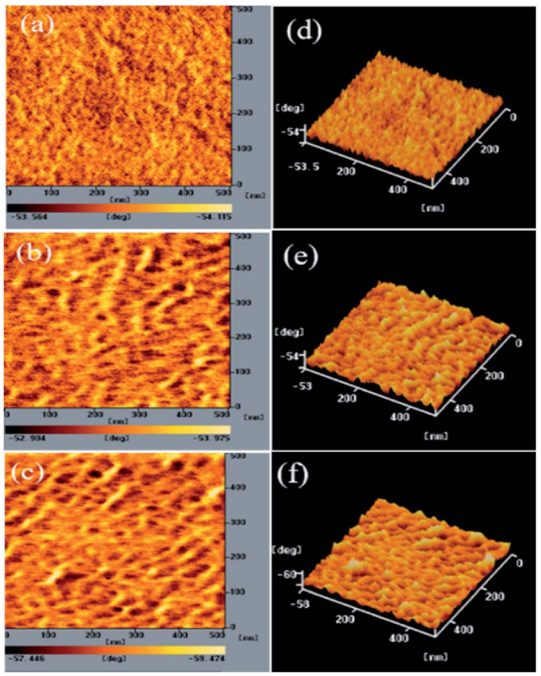

Fig. 6 AFM (tapping mode) (a–c) phase and (d–f) topographic images of **PDPCz11**/$PC_{71}BM$ blend films [(a and d) 1 : 1, w/w; (b and e) 1 : 2, w/w; (c and f) 1 : 3, w/w], recorded after annealing at 100 °C for 10 min.

interpenetrating networks with $PC_{71}BM$-based sizable domains were formed in the composite films after their annealing at 100 °C for 10 min. The $PC_{71}BM$-based electron-transporting channels would presumably favor the electron transfer to the Ca/Ag-based cathode, whereas **PDPCz21** formed interconnecting channels (white areas) that would presumably be favorable for hole transport to the ITO-based anode. Similar TEM images were obtained for the **PDPCz11**/$PC_{71}BM$ blend films (Fig. 8).

3.5 PV properties of PVCs

Fig. 9 presents the best PV performances of these PVCs; the statistical values of the photoenergy conversion efficiencies (η), along with open-circuit voltages (V_{OC}), short-circuit current densities (J_{SC}), fill factors (FFs), and values of η, are summarized in Table 3. Three runs of PV evaluation tests were performed for each PVC sample. The FF did not change significantly in response to the $PC_{71}BM$ content. Meanwhile, the values of V_{OC}, J_{SC}, and η of PVCs increased upon increasing the $PC_{71}BM$ content. The highest values of V_{OC}, J_{SC}, and η were observed for PVC, as its photoenergy conversion layer, featuring the **PDPCz21**/$PC_{71}BM$ blend film at a weight ratio of 1 : 2. Further, the higher $PC_{71}BM$ contents in the photoenergy conversion layer promoted nanoscale phase-separation with $PC_{71}BM$-based sizable domains, which led to effective charge separation and transfer.[32] Efficient dissociation of excitons and higher degrees of charge collection to the electrode generally lead to PVCs displaying enhanced values of V_{OC}, J_{SC}, and η.[29–31] An excessive $PC_{71}BM$ content does not, however, favor charge transfer or enhance the PV properties of a PVC. The PV performances of the PVCs I-3, II-3, and III-3, based on PT/$PC_{71}BM$ at a weight ratio of

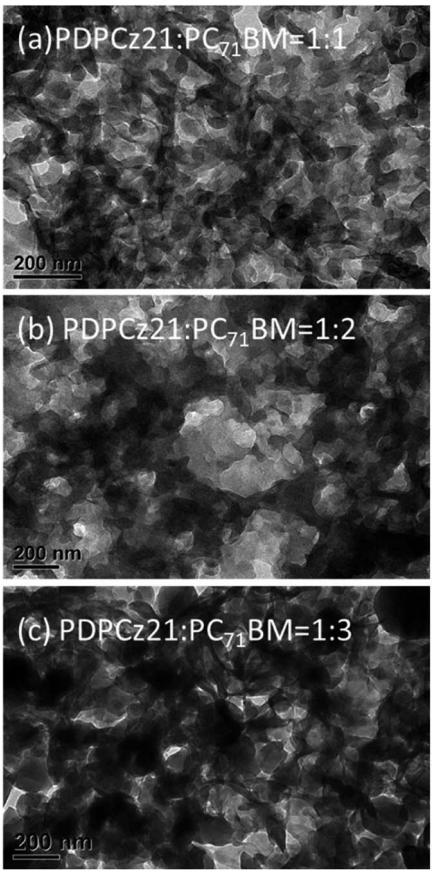

Fig. 7 The TEM images of **PDPCz21**/$PC_{71}BM$ blend solid films after annealing at 100 °C for 10 min.

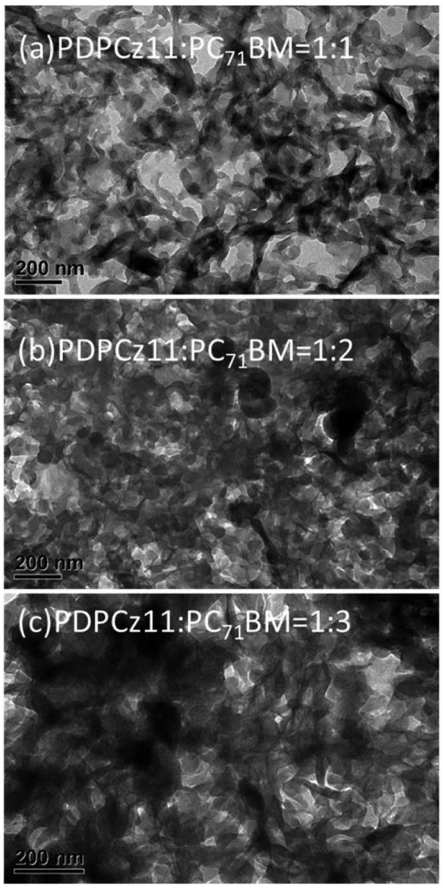

Fig. 8 The TEM images of the **PDPCz11**/$PC_{71}BM$ blend solid films after annealing at 100 °C for 10 min.

1 : 3, were poorer than those of the PVCs I-2, II-2, and III-2, featuring PT/$PC_{71}BM$ at a weight ratio of 1 : 2. Thus, the optimal PT-to-$PC_{71}BM$ ratio was approximately 1 : 2 (w/w) for **PDPP**-, **PDPCz21**-, and **PDPCz11**-based PVCs. On the other hand, the PV properties of the **PDPCz21**- and **PDPCz11**-based PVCs were superior to those of the **PDPP**-based PVCs, reflecting the poorer solubility of **PDPP** and the poorer surface morphologies of the **PDPP**/$PC_{71}BM$ films. In addition, the hole mobilities of the PT/$PC_{71}BM$ blend films were measured using the space-charge limited current method and a typical hole-only device structure of ITO/PEDOT/PT:$PC_{71}BM$/Au.[53] Fig. S4† presents the current densities (J) plotted with respect to the voltage (V). The hole mobility of 1 : 2 (w/w) **PDPCz21**/$PC_{71}BM$ blend film (2.34×10^{-5} cm^2 V^{-1} s^{-1}) was greater than those of 1 : 2 (w/w) **PDPPP**/$PC_{71}BM$ (1.23×10^{-5} cm^2 V^{-1} s^{-1}) and **PDPCz11**/$PC_{71}BM$ (1.96×10^{-5} cm^2 V^{-1} s^{-1}) blend films. The relatively higher hole mobility of the **PDPCz21**/$PC_{71}BM$ (1 : 2, w/w) blend film resulted in the better PV performance of PSC II-2. Nevertheless, the hole mobilities of these TDPP-based PTs were not as high as those of other PTs reported previously in the literature.[54] Thus, incorporating bulky TPCz pendants can result in the twisting of the PT backbone and, subsequently, decrease in its conjugation length and charge transfer capacity.[32] Therefore, the values of J_{SC} and η of the PVCs fabricated from these TDPP-based PT/$PC_{71}BM$ blend films were low relative to those reported previously in the literature.[54] In addition, the PTs containing the conjugated terpyridine moieties (**PDPCz21**, **PDPCz11**) could further be complexed to zinc(II) ions to form metallo-supramolecular polymers. Superior PV properties are generally expected for solar cells based on such metallo-supramolecular polymers.[48] Conjugated polymers containing

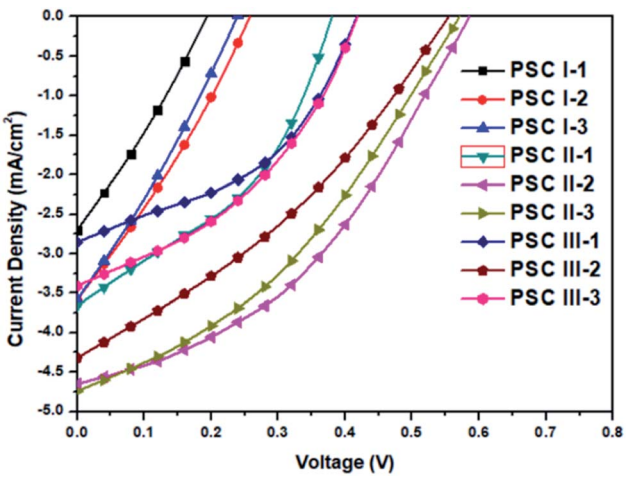

Fig. 9 Current density plotted with respect to potential for illuminated (AM 1.5G, 100 mW cm^{-2}) PVCs based on PT (**PDPP**, **PDPCz21**, **PDPCz11**)/$PC_{71}BM$ composites.

Table 3 Photovoltaic performance of PVCs based on PT (**PDPP**, **PDPCz21**, **PDPCzA11**)/$PC_{71}BM$ composites

PVC	Photoactive layer	PT/$PC_{71}BM$ (w/w)	V_{OC} (V)	J_{SC} (mA cm^{-2})	FF	η (%)	Best η (%)
PVC I-1	**PDPP**/$PC_{71}BM$	1 : 1	0.18 ± 0.02	2.69 ± 0.03	0.26 ± 0.02	0.13 ± 0.03	0.16
PVC I-2	**PDPP**/$PC_{71}BM$	1 : 2	0.23 ± 0.03	3.57 ± 0.02	0.28 ± 0.01	0.23 ± 0.03	0.26
PVC I-3	**PDPP**/$PC_{71}BM$	1 : 3	0.22 ± 0.02	3.58 ± 0.03	0.27 ± 0.02	0.21 ± 0.04	0.25
PVC II-1	**PDPCz21**/$PC_{71}BM$	1 : 1	0.38 ± 0.01	3.67 ± 0.02	0.41 ± 0.01	0.57 ± 0.04	0.61
PVC II-2	**PDPCz21**/$PC_{71}BM$	1 : 2	0.58 ± 0.01	4.59 ± 0.03	0.43 ± 0.01	1.15 ± 0.04	1.19
PVC II-3	**PDPCz21**/$PC_{71}BM$	1 : 3	0.56 ± 0.01	4.71 ± 0.01	0.37 ± 0.01	0.98 ± 0.05	1.03
PVC III-1	**PDPCz11**/$PC_{71}BM$	1 : 1	0.42 ± 0.01	2.85 ± 0.02	0.44 ± 0.01	0.53 ± 0.03	0.56
PVC III-2	**PDPCz11**/$PC_{71}BM$	1 : 2	0.53 ± 0.01	4.31 ± 0.01	0.33 ± 0.01	0.76 ± 0.04	0.82
PVC III-3	**PDPCz11**/$PC_{71}BM$	1 : 3	0.42 ± 0.02	3.41 ± 0.01	0.38 ± 0.01	0.55 ± 0.04	0.59

terpyridine moieties also have potential applications in chemical sensors for detecting metal ions and in light-emitting diodes.[16–19,55] Further modifications of the conjugated PTs containing terpyridine moieties and an investigation of their performance are currently underway.

4. Conclusion

We synthesized three low-band-gap conjugated polymers (**PDPP**, **PDPCz21**, **PDPCz11**) featuring 2-ethylhexyl-functionalized diketopyrrolopyrrole (TDPP) moieties as electron-acceptor units and terpyridine-substituted carbazole (TPCz) moieties as electron-donor units and tested their applicability for use in PVCs. The band gap energies of these polymers increased upon increasing the content of TPCz units. The film quality of the **PDPP**/$PC_{71}BM$ blend films was poor, suggesting high degrees of π-stacking of the TDPP units in the polymer backbone, consistent with the relatively low solubility of **PDPP**. In contrast, the $PC_{71}BM$ units in the **PDPCz21**/$PC_{71}BM$ and **PDPCz11**/$PC_{71}BM$ composite films were distributed uniformly in the polymers. Thus, the **PDPCz21** and **PDPCz11** composite films possessed good film quality, implying that the compatibility of PT and $PC_{71}BM$ was enhanced after the incorporation of the TPCz units in the backbone of the polymer. Incorporating bulky pendants increased the free volume of the PT backbone and, consequently, enhanced the compatibility of PT and $PC_{71}BM$. Therefore, the PV properties of the **PDPCz21**- and **PDPCz11**-based PVCs were superior to those of the **PDPP**-based PVCs.

Conflicts of interest

There are no conflicts to declare.

Acknowledgements

We thank the Ministry of Science and Technology (Most 107-2221-E-005-018) of Taiwan for financial support.

References

1 N. Pilicodea, K. M. Nimith, M. Acharya, P. Naik, M. N. Satyanarayan and A. V. Adhikari, New blue light emitting cyanopyridine based conjugated polymers: from molecular engineering to PLED applications, *J. Photochem. Photobiol., A*, 2019, **378**, 38–45.

2 R. H. Lee and L. W. Liu, Electroluminescence and photovoltaic properties of light-emitting devices and solar cells comprising 2-pyran-4-ylidene-malononitrile conjugated polymers, *Dyes Pigm.*, 2010, **84**, 190–202.

3 D. T. Christiansen, S. Ohtani, Y. Chujo, A. L. Tomlinson and J. R. Reynolds, All donor electrochromic polymers tunable across the visible spectrum *via* random copolymerization, *Chem. Mater.*, 2019, **31**, 6841–6849.

4 F. J. Lin, S. D. Lin, C. H. Chin, W. T. Chuang and C. S. Hsu, Novel conjugated polymers based on bis-dithieno [3,2-*b*;2′,3′-d]pyrrole vinylene donor and diketopyrrolopyrrole acceptor: side chain engineering in organic field effect transistors, *Polym. Chem.*, 2018, **9**, 28–37.

5 H. C. Wu, C. C. Hung, C. W. Hong, H. S. Sun, J. T. Wang, G. Yamashita, T. Higashihara and W. C. Chen, Isoindigo-based semiconducting polymers using carbosilane side chains for high performance stretchable field-effect transistors, *Macromolecules*, 2016, **49**, 8540–8548.

6 K. E. Hung, C. E. Tsai, S. L. Chang, Y. Y. Lai, U. S. Jeng, F. Y. Cao, C. S. Hsu, C. J. Su and Y. J. Cheng, Bispentafluorophenyl-containing additive: enhancing efficiency and morphological stability of polymer solar cells *via* hand-grabbing-like supramolecular pentafluorophenyl–fullerene interactions, *ACS Appl. Mater. Interfaces*, 2017, **9**, 43861–43870.

7 N. Zhou, A. S. Dudnik, T. I. N. G. Li, E. F. Manley, T. J. Aldrich, P. Guo, H. C. Liao, Z. Chen, L. X. Chen, R. P. H. Chang, A. Facchetti, M. O. D. L. Cruz and T. J. Marks, All-polymer solar cell performance optimized *via* systematic molecular weight tuning of both donor and acceptor polymers, *J. Am. Chem. Soc.*, 2016, **138**, 1240–1251.

8 Q. Fan, Q. Zhu, Z. Xu, W. Su, J. Chen, J. Wu, X. Guo, W. Ma, M. Zhang and Y. Li, Chlorine substituted 2D-conjugated polymer for high-performance polymer solar cells with 13.1% efficiency *via* toluene processing, *Nano Energy*, 2018, **48**, 413–420.

9 Y. Huo, J. Zhu, X. Z. Wang, C. Yan, Y. F. Chai, Z. Z. Chen, X. Zhan and H. L. Zhang, Small molecule donors based on benzodithiophene and diketopyrrolopyrrole compatible with both fullerene and non-fullerene acceptors, *J. Mater. Chem. C*, 2018, **6**, 5843–5848.

10 M. Privado, P. D. L. Cruz, S. Biswas, R. Singhal, G. D. Sharma and F. Langa, A non-fullerene all small molecule solar cell constructed with a diketopyrrolopyrrole-based acceptor having a power conversion efficiency higher than 9% and an energy loss of 0.54 eV, *J. Mater. Chem. A*, 2018, **6**, 11714–11724.

11 Y. Xie, Y. Yu, Q. Liang, J. H. Wan, H. Wu and Y. Cao, Understanding the enhanced open-circuit voltage of polymer solar cells based on a diketopyrrolopyrrole small molecular acceptor, *ACS Appl. Mater. Interfaces*, 2018, **10**, 25589–25593.

12 H. Sun, T. Liu, J. Yu, T. K. Lau, G. Zhang, Y. Zhang, M. Su, Y. Tang, R. Ma, B. Liu, J. Liang, K. Feng, X. Lu, X. Guo, F. Gao and H. Yan, A monothiophene unit incorporating both fluoro and ester substitution enabling high-performance donor polymers for non-fullerene solar cells with 16.4% efficiency, *Energy Environ. Sci.*, 2019, **12**, 3328–3337.

13 C. Zhao, Y. Guo, Y. Zhang, N. Yan, S. You and W. Li, Diketopyrrolopyrrole-based conjugated materials for non-fullerene organic solar cells, *J. Mater. Chem. A*, 2019, **7**, 10174–10199.

14 J. L. Wu, C. W. Lin, J. Golder, T. W. Lin, C. T. Chen and C. T. Chen, Oligothiophenes and alkyl side-chain arrangement the structure-property study of their diketopyrrolopyrrole copolymers for organic photovoltaics, *Org. Electron.*, 2018, **61**, 185–196.

15 C. Li, C. Yu, W. Lai, S. Liang, X. Jiang, G. Feng, J. Zhang, Y. Xu and W. Li, Multifunctional diketopyrrolopyrrole-based conjugated polymers with perylenebisimide side chains, *Macromol. Rapid Commun.*, 2018, **39**, 1700611.

16 P. C. Yang, D. S. Q. Li, Y. H. Chien, T. L. Tao, R. Y. Huang and H. Y. Chen, Synthesis, chemosensory properties, and self-assembly of terpyridine-containing conjugated polycarbazole through RAFT polymerization and Heck coupling reaction, *Polymers*, 2017, **9**, 427.

17 R. S. Juang, P. C. Yang, H. W. Wen, C. Y. Lin, S. C. Lee and T. W. Chang, Synthesis and chemosensory properties of terpyridine-containing diblock polycarbazole through RAFT polymerization, *React. Funct. Polym.*, 2015, **93**, 130–137.

18 P. C. Yang, H. W. Wen, C. W. Huang and Y. N. Zhu, Synthesis and chemosensory properties of two-arm truxene-functionalized conjugated polyfluorene containing terpyridine moiety, *RSC Adv.*, 2016, **6**, 87680–87689.

19 H. Zhang, K. Yang, C. Chen, Y. Wang, Z. Zhang, L. Tang, Q. Sun, S. Xue and W. Yang, 1,4-Diketo-pyrrolo[3,4-*c*] pyrroles (DPPs) based insoluble polymer films with lactam hydrogens as renewable fluoride anion chemosensor, *Polymer*, 2018, **149**, 266–272.

20 M. Zhang, L. Zhu, P. Guo, X. Wang, J. Tong, X. Zhang, Y. Jia, R. Yang, Y. Xia and C. Wang, Effect of flank rotation on the photovoltaic properties of dithieno[2,3-*d*:2′,3′-*d*′]benzo[1,2-*b*:4,5-*b*′]dithiophene-based narrow band gap copolymers, *Polymers*, 2019, **11**, 239.

21 C. Li, C. Yu, W. Lai, S. Liang, X. Jiang, G. Feng, J. Zhang, Y. Xu and W. Li, Multifunctional diketopyrrolopyrrole-based conjugated polymers with perylenebisimide side chains, *Macromol. Rapid Commun.*, 2018, **39**, 1700611.

22 Y. Zhang, X. Li, T. Dai, D. Xu, J. Xi and X. Chen, Charge transport and extraction of PTB7:PC71BM organic solar cells: Effect of film thickness and thermal-annealing, *RSC Adv.*, 2019, **9**, 24895–24903.

23 C. Cui, W. Y. Wong and Y. F. Li, Improvement of open-circuit voltage and photovoltaic properties of 2D-conjugated polymers by alkylthio substitution, *Energy Environ. Sci.*, 2014, **7**, 2276–2284.

24 G. H. Lim, K. S. Lee, Y. J. Park, J. Shim, J. W. Choi, M. Kim, Y. Jin, B. Lim, Y. Yi, C. L. Lee, J. Y. Hwang and D. I. Son, Charge transport effect and photovoltaic conversion of two-dimensional CdSeS quantum dot monolayers in inverted polymer solar cells, *J. Mater. Chem. C*, 2019, **7**, 11797–11805.

25 G. Kocak, D. Gedefaw and M. R. Andersson, Optimizing polymer solar cells using non-halogenated solvent blends, *Polymers*, 2019, **11**, 544.

26 J. A. Khan, R. Sharma, S. K. Sarkar, A. S. Panwar and D. Gupta, Combined effect of ZnO nanoripples and solvent additive on the nanomorphology and performance of PTB7-Th:$PC_{71}BM$ organic solar cells, *Nanotechnology*, 2019, **30**, 385204.

27 R. Heuvel, F. J. M. Colberts, J. Li, M. M. Wienkac and R. A. Janssen, The effect of side-chain substitution on the aggregation and photovoltaic performance of diketopyrrolopyrrole-alt-dicarboxylic ester bithiophene polymers, *J. Mater. Chem. A*, 2018, **6**, 20904–20915.

28 W. H. Lee, B. T. Liu and R. H. Lee, Difluorobenzothiadiazole based two-dimensional conjugated polymers with triphenylamine substituted moieties as pendants for bulk heterojunction solar cells, *eXPRESS Polym. Lett.*, 2017, **11**, 910–923.

29 Y. Shi, Y. Tang, K. Yang, M. Qin, Y. Wang, H. Sun, M. Su, X. Lu, M. Zhou and X. Guo, Thiazolothienyl imide-based wide band gap copolymers for efficient polymer solar cells, *J. Mater. Chem. C*, 2019, **7**, 11142–11151.

30 B. Xu, G. Saianand, V. A. L. Roy, Q. Qiao, K. M. Reza and S. W. Kang, Employing PCBTDPP as an efficient donor polymer for high performance ternary polymer solar cells, *Polymers*, 2019, **11**, 1423.

31 H. Chen, G. Cai, A. Guo, Z. Zhao, J. Kuang, L. Zheng, L. Zhao, J. Chen, Y. Guo and Y. Liu, Low band gap donor–acceptor conjugated polymers with indanone-condensed thiadiazolo [3,4-*g*]quinoxaline acceptors, *Macromolecules*, 2019, **52**, 6149–6159.

32 H. J. Wang, J. Y. Tzeng, C. W. Chou, C. Y. Huang, R. H. Lee and R. J. Jeng, Novel polythiophene derivatives functionalized with conjugated side-chain pendants comprising triphenylamine/carbazole moieties for photovoltaic cell applications, *Polym. Chem.*, 2013, **4**, 506.

33 L. Yang, Y. Yu, J. Zhang, F. Chen, X. Meng, Y. Qiu, Y. Dan and L. Jiang, In-situ fabrication of diketopyrrolopyrrole-carbazole-based conjugated polymer/TiO_2 heterojunction for enhanced visible light photocatalysis, *Appl. Surf. Sci.*, 2018, **434**, 796–805.

34 X. Li, K. Wu, L. Zheng, Y. Deng, S. Tan and H. Chen, Synthesis and characterization of novel benzodithiophene-fused perylenediimide acceptors: regulate photovoltaic performance *via* structural isomerism, *Dyes Pigm.*, 2019, **168**, 59–67.

35 F. Li, X. Song, K. Zhang, B. Shahid, Q. Wang, L. Yu, D. Zhuc and M. Sun, Carbazole side-chained benzodithiophene based two-dimensional D–A conjugated photovoltaic polymers, *Dyes Pigm.*, 2019, **170**, 107548.

36 P. Zhou, D. Dang, J. Fan, W. Xiong, C. Yang, H. Tan, Y. Wang, Y. Liu and W. Zhu, Increasing thiophene spacers between thieno[3,2-*b*]thiophene and benzothiadiazole units in backbone to enhance photovoltaic performance for their 2-D polymers, *Dyes Pigm.*, 2015, **112**, 99–104.

37 K. Kranthiraja, K. Gunasekar, W. Cho, M. Song, Y. G. Park, J. Y. Lee, Y. Shin, I. N. Kang, A. Kim, H. Kim, B. Kim and S. H. Jin, Alkoxyphenylthiophene linked benzodithiophene based medium band gap polymers for organic photovoltaics: efficiency improvement upon methanol treatment depends on the planarity of backbone, *Macromolecules*, 2014, **47**, 7060–7069.

38 M. L. Keshtov, S. A. Kuklin, I. O. Konstantinov, I. E. Ostapov, D. Y. Godovsky, E. E. Makhaeva, Z. Xie and G. D. Sharma, Conjugated random terpolymers based on benzodithiophene, diketopyrrolopyrrole, and 8,10-bis(thiophen-2-yl)-2,5-di(nonadecan-3-yl)bis [1,3]thiazolo [4,5-*f*:50,40-*h*]thieno[3,4-*b*]quinoxaline for efficient polymer solar cell, *J. Polym. Sci., Part A: Polym. Chem.*, 2019, **57**, 1478–1485.

39 A. Domokos, S. D. Aronow, T. Tang, N. E. Shevchenko, D. J. Tantillo and A. S. Dudnik, Synthesis and optoelectronic properties of new methoxy-substituted diketopyrrolopyrrole polymers, *ACS Omega*, 2019, **4**, 9427–9433.

40 A. Negash, Z. Genene, R. T. Eachambadi, J. Kesters, N. V. D. Brande, J. D'Haen, H. Penxten, B. A. Abdulahi, E. Wang, K. Vandewal, W. Maes, W. Mammo, J. Mancad and S. Admassiea, Diketopyrrolopyrrole-based terpolymers with tunable broad band absorption for fullerene and fullerene-free polymer solar cells, *J. Mater. Chem. C*, 2019, **7**, 3375–3384.

41 H. J. Kim, M. Pei, J. S. Ko, M. H. Ma, G. E. Park, J. Baek, H. Yang, M. J. Cho and D. H. Choi, Influence of branched alkyl ester-labeled side chains on specific chain arrangement and charge-transport properties of diketopyrrolopyrrole-based conjugated polymers, *ACS Appl. Mater. Interfaces*, 2018, **10**, 40681–40691.

42 D. Dang, P. Zhou, Q. Peng, K. He, H. Jiang, P. Yang, H. Tan, Y. Wang, Y. Liu, G. Lei and W. Zhu, Improved photovoltaic performance of two-dimensional low band-gap conjugated polymers with thieno[3,2-*b*]thiophene and diketopyrrolopyrrole units by altering pendent position of conjugated side chain, *Dyes Pigm.*, 2014, **109**, 6–12.

43 H. Liang, X. Zhang, R. Peng, X. Ouyang, Z. Liu, S. Chen and Z. Ge, Photovoltaic performance enhancement from diketopyrrolopyrrole-based solar cells through structure manipulation, *Dyes Pigm.*, 2015, **112**, 145–153.

44 G. Zhang, Y. Fu, Z. Xie and Q. Zhang, Synthesis of low band gap polymer based on 3,6-dithien-2-yl-2,5-dialkylpyrrolo[3,4-*c*]pyrrole-1,4-dione for photovoltaic applications, *Sol. Energy Mater. Sol. Cells*, 2011, **95**, 1168–1173.

45 C. Buckley, S. Thomas, M. McBride, Z. Yuan, G. Zhang, J. L. Bredas and E. Reichmanis, Synergistic use of bithiazole and pyridinyl substitution for effective electron transport polymer materials, *Chem. Mater.*, 2019, **31**, 3957–3966.

46 K. Aoshima, M. Nomura and A. Saeki, Regioregularity and electron deficiency control of unsymmetric diketopyrrolopyrrole copolymers for organic photovoltaics, *ACS Omega*, 2019, **4**, 15645–15652.

47 G. Qiu, Z. Jiang, Z. Ni, H. Wang, H. Dong, J. Zhang, X. Zhang, Z. Shu, K. Lu, Y. Zhen, Z. Wei and W. Hu, Asymmetric thiophene/pyridine flanked diketopyrrolopyrrole polymers for high performance polymer ambipolar field-effect transistors and solar cells, *J. Mater. Chem. C*, 2017, **5**, 566–572.

48 X. Chen, K. Guo, F. Li, L. Zhou and H. Qiao, Synthesis and properties of Zn^{2+}/Cd^{2+}-directed self-assembled metallo-supramolecular polymers based on 1,4-diketo-pyrrolo[3,4-*c*]pyrrole (DPP) derivatives, *RSC Adv.*, 2014, **4**, 58027–58035.

49 H. Liang, X. Zhang, R. Peng, X. Ouyang, Z. Liu, S. Chen and Z. Ge, Photovoltaic performance enhancement from diketopyrrolopyrrole-based solar cells through structure manipulation, *Dyes Pigm.*, 2015, **112**, 145–153.

50 H. J. Wang, Y. P. Chen, Y. C. Chen, C. P. Chen, R. H. Lee, L. H. Chan and R. J. Jeng, Synthesis and photovoltaic properties of two-dimensional conjugated polythiophene derivatives presenting conjugated triphenylamine/thiophene moieties, *Polymer*, 2012, **53**, 4091–4103.

51 S. Y. Shiau, C. H. Chang, W. J. Chen, H. J. Wang, R. J. Jeng and R. H. Lee, Star-shaped organic semiconductors with planar triazine core and diketopyrrolopyrrole branches for solution-processed small-molecule organic solar cells, *Dyes Pigm.*, 2015, **115**, 35–49.

52 Y. Li and Y. Zou, Conjugated polymer photovoltaic materials with broad absorption band and high charge carrier mobility, *Adv. Mater.*, 2008, **20**, 2952–2958.

53 C. Y. Huang, W. H. Lee and R. H. Lee, Solution processable star-shaped molecules with a triazine core and branching thienylenevinylenes for bulk heterojunction solar cells, *RSC Adv.*, 2014, **4**, 48150–48162.

54 Z. Deng, T. Ai, R. Li, W. Yuan, K. Zhang, H. Du and H. Zhang, Conjugated polymers containing building blocks 1,3,4,6-tetraarylpyrrolo[3,2-*b*]pyrrole-2,5-dione (isoDPP), benzodipyrrolidone (BDP) or naphthodipyrrolidone (NDP): a review, *Polymers*, 2019, **11**, 1683.

55 H. Sasabe, Y. Hayasaka, R. Komatsu, K. Nakao and J. Kido, Highly luminescent p-conjugated terpyridine derivatives exhibiting thermally activated delayed fluorescence, *Chem.–Eur. J.*, 2017, **23**, 114–119.